IEEE Access
Multidisciplinary | Rapid Review | Open Access Journal

Received July 19, 2019, accepted July 29, 2019, date of publication August 1, 2019, date of current version August 15, 2019.

*Digital Object Identifier 10.1109/ACCESS.2019.2932468*

# Benchmarking a High-End Smartphone's Antenna Efficiencies

**LAURENS A. BRONCKERS, (Student Member, IEEE), ANNE ROC'H, (Member, IEEE), AND A. BART SMOLDERS, (Member, IEEE)**
Department of Electrical Engineering, Eindhoven University of Technology, 5600MB Eindhoven, The Netherlands
Corresponding author: Laurens A. Bronckers (l.a.bronckers@tue.nl)

This work was supported in part by the Aeneas/Catrene Project EAST.

**ABSTRACT** In an effort to create a benchmark for antenna designs for mobile applications, the total and radiation efficiencies of a modern high-end smartphone's antennas are measured. To this end, an adapter board is designed that facilitates the connection to a calibrated measurement system. Its shape is chosen to closely resemble the original phone's dimensions while allowing connection of the antennas via spring fingers to a coaxial measurement system. The characterization of this mock-up is performed in a reverberation chamber, which offers the advantage of an on-average isotropic environment, making it ideal for antenna reflection coefficient and efficiency measurements. The reflection coefficients, total efficiencies, and radiation efficiencies of the mock-up are then measured from 0.75 to 6 GHz. The total antenna efficiencies, not accounting for a possible improvement due to adaptive matching networks, are found to be below 15% up to 4 GHz and up to 25% below 6 GHz. Meanwhile, the radiation efficiencies are up to 15% below 2.5 GHz and up to 40% below 6 GHz. Such antenna efficiency measurements are the first and serve well as a benchmark for future designs and concepts.

**INDEX TERMS** Antenna efficiency measurements, reverberation chambers, smartphone antennas.

## I. INTRODUCTION

Modern smartphones, especially the high-end models, have shown a clear trend towards thinner designs and higher integration. At the same time, 5G will make use of even more available frequency space in the 1 to 6 GHz range than 4G [1]–[5]. One may wonder in what position this leaves an antenna designer, confronted with the challenge of creating a robust and cheaply manufacturable design within very limited available real estate. On the one hand, the radiation pattern is not of critical concern (though the specific absorption rate (SAR) is) due to the scattering environment the phone is designed for, and the input impedance can be improved using adaptive matching circuits. On the other hand the antenna efficiencies have a direct impact on the link budget and thereby battery life and maximum bit rate.

Since it is such a critical parameter, the antenna efficiency performance of state-of-the-art models could very well serve as a benchmark for new concepts and designs. However, very few characterizations of commercial designs, especially recent high-end models, can be found in literature [6]–[10].

The associate editor coordinating the review of this manuscript and approving it for publication was Bora Onat.

The influence of head and hand on the radiation efficiencies are studied in [6], [7], [9], but these were not smartphones and included relatively large antennas. A study on the effect of phone-chassis related parameters on, among others, the antenna efficiency was performed in [8], but this did not include a commercial design where cost and form-factor are the primary drivers for the antenna topology and geometry. In 2012, a very thorough analysis of a phone's antenna performance was performed [10], presenting challenges on the antenna performance for then-current designs. However, the antenna efficiencies were not studied separately, and the form factor as well as functionality of smartphones have evolved significantly since then. Most other existing work focuses on the electronics or the complete phone, where the antenna's contribution to the overall performance cannot be distinguished from the electronics [11]–[14]. This may in part be attributed to the difficulty of accurately measuring antenna efficiencies, and practical issues that prevent the antennas from being directly connected to the measurement system. Therefore, the antenna community has focused on creating and characterizing new designs, designing for and measuring the antenna efficiencies as well [15]–[19]. While it has been shown that these antennas, often frequency-reconfigurable,


This work is licensed under a Creative Commons Attribution 4.0 License. For more information, see http://creativecommons.org/licenses/by/4.0/

can perform well, it is as yet unclear how they compare to the current state-of-the-art in commercially available smartphones.

Recently, three reverberation chamber (RC) methods were proposed that make the procedure of measuring antenna efficiency possible without the need for a reference antenna [20]. In this work, we apply the three-antenna method (which makes the smallest amount of assumptions on the RC) to measure the efficiencies of the antennas in a very popular high-end smartphone with a screen folding around the edges, first introduced in 2017. Its most crucial properties are the large screen, posing increasing challenges to the antenna systems, and its support of LTE Cat-16, one of the highest grades in the 3GPP LTE standard [21]. Such a phone is selected for its stringent requirements on a system level, resulting in extremely challenging form-factor and placement limitations for the antennas. The practical impact of such requirements has yet to be shown in literature. To solve the problem of connecting the antenna to the measurement system, we have designed a special adapter board to adapt the spring-finger connection of the original phone to an SMA connector interface. We then measure this mock-up's antennas in a reverberation chamber. The results of these measurements are extremely valuable to serve as a reference (or benchmark) of an industry design that we deem to be representative due to its large popularity, to compare new antenna designs and concepts.

We start by detailing the way the phone is constructed, where the antennas can be found and what their most likely purpose is. We then describe the design of the adapter board to connect the antennas to the measurement systems. This is followed by descriptions of the measurement setup in Section IV, where we provide and discuss the measurement results as well. The work is concluded in Section V.

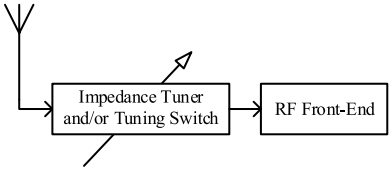


**FIGURE 1.** Block diagram of common antenna connection to the RF front-end: an impedance tuner is included at the antenna connection.

## II. ANTENNAS AND RF FRONT-END

Before proceeding to the design of the adapter board to allow for antenna testing, we first take a look at the way the antennas are integrated in the smartphone. A common configuration is to connect an impedance tuner between the antenna and the RF front-end [22], as illustrated in Figure 1. Sometimes this tuner takes the form of a switch between different filters and/or matching networks. The inclusion of such a network has several advantages to the overall design: one can compensate for impedance mismatches introduced by the user, and impedances different from the 50 Ω that is commonly required for maximum power transfer [23] can be accepted at the antenna port. In other words, the antenna is no longer required to present 50 Ω. The impedance range that can be matched varies per (often proprietary or custom designed) adaptive impedance tuner, info about which proved unfeasible for us to obtain. The tuners are frequently integrated with other front-end functionalities. Observing the two commonly defined antenna efficiencies, the total efficiency ($\eta_{\text{tot}} = P_{\text{radiated}}/P_{\text{available}}$, the ratio of the available and radiated powers) and the radiation efficiency ($\eta_{\text{rad}} = P_{\text{radiated}}/P_{\text{accepted}}$, the ratio of the accepted and radiated powers), the matching circuit only influences the total efficiency. The radiation efficiency can be viewed as an upper limit for the total efficiency, representing the hypothetical case where the antenna is perfectly matched. Thus, even if the impedance tuners are not included in a measurement, the radiation efficiency is still representative for the antenna performance in the final application.


**FIGURE 2.** The smartphone partly disassembled. The antennas (a) consist of metallization on two pieces of plastic, that are normally mounted in the same orientation to the rest of the phone (b). The phone's boards connect to the antennas using spring fingers.

In modern smartphones, conventional (coaxial) connectors are no longer used for most antenna connections. Instead, the antenna elements connect to the (main) board via spring fingers. This smartphone (Figure 2) is one that uses such an approach: the antenna layer (Figure 2(a)) is screwed on top of the phone with main and sub board (Figure 2(b)), pressing the antennas to spring fingers on the PCB's. The only layer that follows on top of that is the phone's back cover. Five distinctly connected antennas can be found on the antenna layer. It is challenging to derive any definitive conclusion about their functionality, especially with a phone that supports many standards and bands such as the one tested here: it supports bands in the 700-900 MHz range (low LTE bands), 1800-2100 MHz range (mid LTE bands), 2.3-2.6 GHz range (high LTE bands) and 3.5 GHz bands, as well as 2.4 GHz and 5 GHz WiFi, Bluetooth and GPS.

However, from the connected electronics we can deduce, following the numbering of Figure 2(a):

1) **GPS** antenna, with an unfolded length of approximately 30 mm.
2) **Sub** antenna; the total unfolded length of this element is approximately 40 mm.
3) **Bluetooth/WiFi** antenna; the total length of the two arms together is approximately 20 mm, with an additional arm that is approximately 7 mm long.
4) **Bluetooth/WiFi** antenna with a total unfolded length of approximately 20 mm.
5) **Main** antenna; this inverted-L antenna with a stub close to the feed is approximately 21 mm long (unfolded).

The GPS and Bluetooth/WiFi appear to be used exclusively for those purposes. The 'main' antenna seems to be used for the mid and high LTE bands, as well as legacy (2G) mobile communications. The sub antenna appears to be used for the low LTE bands, as well as diversity for the mid and high LTE bands. Antennas 3 and 4 are connected through lines and components on the circuit board, most likely intended to combine them towards a single feed. As the topology behind this is unknown to us, we will test them with individual feeds. In the rest of this paper, we will use the above antenna numbering, as opposed to using their (most likely) functionality. Therefore the validity of the results does not depend on them. We will now investigate how we can connect the antennas to a measurement system.

## III. ADAPTER BOARD

Due to the size of the electronics and traces on the board, accessing the transmission lines coming from the antennas with a measurement system is very challenging. Therefore we decide to keep only the antennas and back cover, and replace the rest of the phone by a PCB that provides a transition from the antennas to a measurement system. We will refer to this PCB as the adapter board. To closely resemble a mass-production situation, FR-4 PCB material is chosen as substrate. The overall dimensions of the adapter board are chosen to match those of the phone (approximately 150 x 68 mm), as it is known that the phone's chassis can contribute significantly to the overall radiation [24]–[26], with a thickness of 1.6 mm. The adapter board, with the antennas and back cover installed, is shown in Figure 3(a) and 3(b) from the front and back, respectively. This will be referred to as the mock-up. Modifications to the original phone's parts are kept to a minimum, only creating additional holes (to allow for plastic bolts required to mount the parts) well away from the antennas. The copper area on the bottom right of the rear side is necessitated by a protrusion of the plastic antenna layer, requiring a cutout in the PCB. The copper is there to ensure that currents can run uninterrupted to the corner of the original phone. Each of the SMA connectors transitions to a coplanar waveguide with ground (GCPW) running on the back side with vias to prevent odd modes and radiation, as well as providing an uninterrupted path for currents

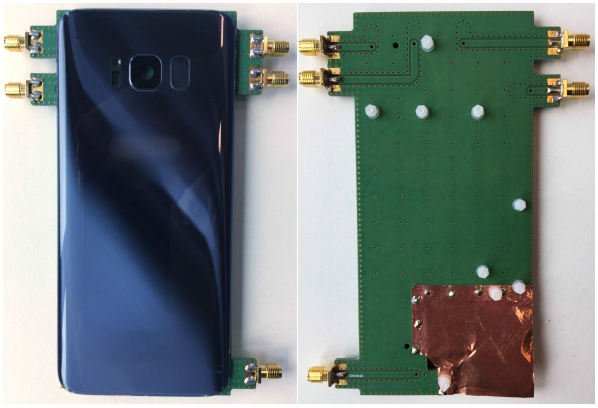


**FIGURE 3.** Smartphone mock-up, front view (a) and rear view (b). As during all measurements, the original cover is placed over the adapter board with antennas. If one were to take off the cover of (a), one would see the antennas exposed as in Figure 2(a).

on each side of the ground plane. The GCPW, with a gap width of 0.75 mm and a center conductor width of 2.4 mm, is created on the back side of the board so that it is not influenced by the dielectric parts of the phone. As close as possible to the antenna element, the GCPW is fed through the board using a via, connecting to a spring finger of a similar type as used in the original phone. Detailed views of the original connection and our replacement are shown in Figures 4 and 5, respectively.

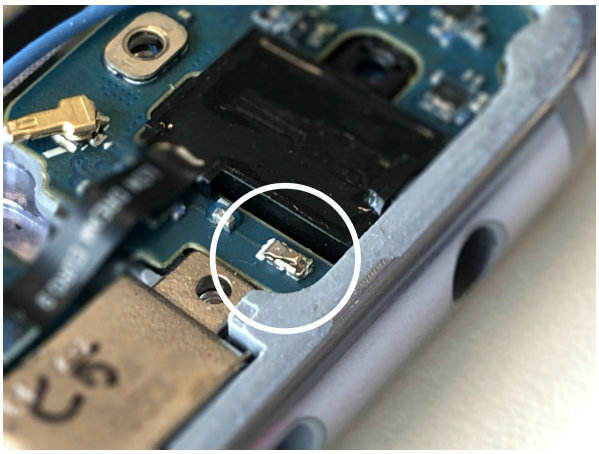

**FIGURE 4.** Detailed view of an original antenna connection in the phone.

In order to ensure that the transmission lines, and especially the transitions from coax to GCPW on the adapter board, does not significantly impact the measurement results, we verified this part of the system separately. Instead of using simulations and thereby making assumptions on the material properties of the board (which are not accurately known for FR-4), we design a board using the exact same GCPW line and transition to SMA, but with an identical connection on the other side, as shown in Figure 7. The total length of the board is 4 cm, so assuming symmetry half the insertion loss of this

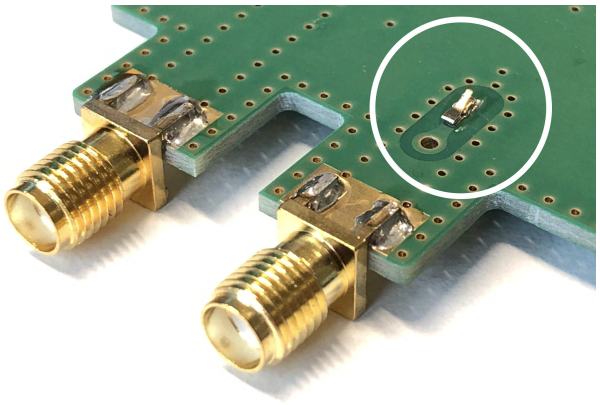

**FIGURE 5.** Our replacement for the spring finger of Figure 4, where we can see an SMA connector, transitioning to the spring finger using a GCPW on the rear side of the board.

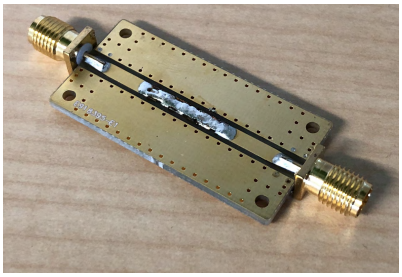

**FIGURE 6.** Photograph of the GCPW thru-connection board. The dimensions and materials are the same as used on the designed phone board.

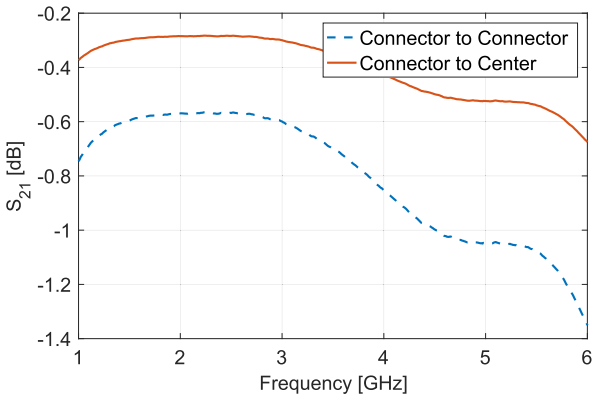


**FIGURE 7.** Measurement of the GCPW thru-connection board. The connector-to-connector insertion loss dips just below 1.2 dB at 5.5 GHz, translating to an insertion loss just below 0.6 dB from one connector interface to the center of the board.

board corresponds to one SMA connector with a transition and line of 2 cm. The results for this half of the test board show a maximum insertion loss of approximately 0.7 dB at 6 GHz. It seems reasonable to assume that the lines and transitions on the original phone boards, with their extremely tight space restrictions, exhibit at least similar losses. Note that the insertion losses measured on our test board correspond to an efficiency in power transfer above 93%. Therefore this could introduce a relative error of at most 7% in the final result, e.g. a 1.4% deviation for an antenna efficiency of 20%. Combined with the argument of transmission lines being present on the original boards feeding the antennas as well, we decided to neglect the effects of these transmission lines for the rest of the study.

## IV. MEASUREMENTS

### A. MEASUREMENT SETUP

The antenna efficiencies are measured using the three-antenna method introduced in [20]. This method uses a reverberation chamber, which can be described as a large metal cavity with a metal stirrer in it to perturb the fields. By changing the stirrer's position, followed by averaging in post-processing, an *on average* uniform field distribution can be obtained. Traditionally, reverberation chambers have been used mainly for electromagnetic compatibility applications, while anechoic chambers were applied for antenna and communication measurements. More recently however, antenna efficiency measurements in reverberation chambers [20], [27]–[35] have emerged. One of the advantages when compared to anechoic chambers is that there is no need for device alignment or three-dimensional scans, as the angular dependence is averaged out. This offers an ideal environment for the testing of isotropic parameters, such as antenna efficiencies. In addition, the three-antenna method does not require a reference antenna, but instead uses the reverberation chamber's time constant to model the empty chamber's losses, enabling one to calculate the antenna efficiencies. It makes use of three antennas ($A$, $B$ and $C$), measured in pairs at a time in the reverberation chamber. As an example the total efficiency of antenna A can be calculated using

$$\eta_{\text{tot,A}} = \sqrt{\frac{C_{\text{RC}}}{\omega}}\sqrt{\frac{M_{AB}M_{AC}}{M_{BC}}}, \tag{1}$$

where

$$C_{\text{RC}} = \frac{16\pi^2 V}{\lambda^3} \tag{2}$$

$$M_{ij} = \frac{\langle |S_{21,s}|^2 \rangle_{ij}}{\tau_{\text{RC}}}, \tag{3}$$

where $i$ and $j$ are antenna $A$, $B$ or $C$, $\tau_{\text{RC}}$ is the chamber's time-constant derived from its' power-delay profile, the $s$ subscript on the S-parameters indicate the S-parameters corrected for un-stirred energy, and $\langle\cdot\rangle$ indicates averaging over the defined frequency band and paddle positions. The three-antenna method is the most robust of the different antenna efficiency measurement methods proposed in [20], since it makes the smallest amount of assumptions and uses only the transmission S-parameters. For details on the procedure and the calculation, we refer the reader to [20] as an extended description is outside the scope of this paper.

The reverberation chamber's dimensions are $4.05 \times 5.70 \times 3.15$ m$^3$, and it uses a moving-wall type of stirrer [36],

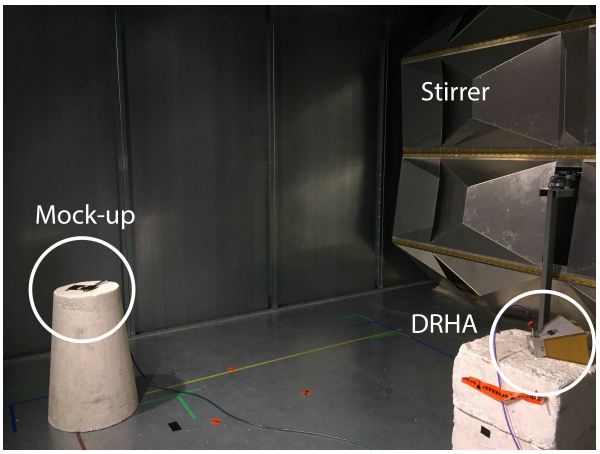


**FIGURE 8.** Setup of the antenna measurements in the reverberation chamber. The DRHA measurement antenna is positioned on the right, with the mock-up on the styrofoam on the left.

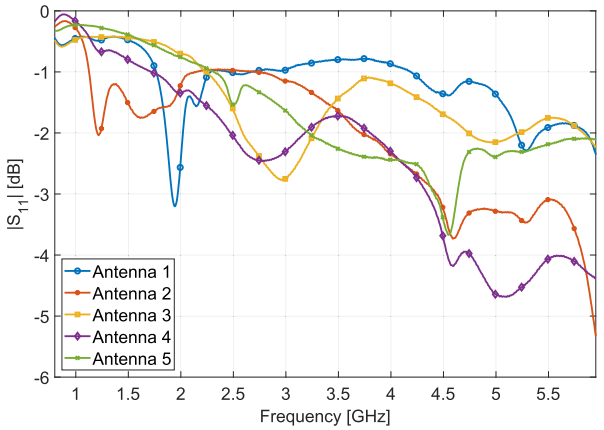


**FIGURE 9.** Measurement of the antenna reflection coefficients with the board. Due to the presence of an adaptive matching network at the antenna connector, the antenna is not required to be self-matched.

as shown in Figure 8. The measurement antennas are dual-ridged horn antennas (DRHAs), an EMCO model 3115 [37] and a Com-power AH-118 [38], which can both cover the 0.75-18 GHz range. In a reverberation chamber, it is important to minimize the direct coupling between the antennas in order to maximize the amount of energy interacting with the stirrer. Therefore the directional DRHA is pointed at the moving wall. The antennas are both positioned well-away from any conducting surface, to avoid disturbing the antenna behaviors. Apart from this these effects, which we alleviate by using one highly directive DRHA, the radiation patterns do not influence the measurement results in the reverberation chamber. We take $N = 100$ mode-stirring samples, with 100 MHz frequency stirring. Both antennas are connected to a VNA outside the reverberation chamber using phase-stable cables with a 3.5 mm connector interface. We use a frequency step of 250 kHz and cover a range of 750 MHz to 6 GHz with a VNA IF Bandwidth of 1 kHz and 0 dBm output power. Therefore we have 40.000 samples per center frequency point for the efficiency calculation. The setup is calibrated at a 3.5 mm interface, avoiding the inclusion of any adaptors in the measurement. A comparison between the efficiencies obtained using this chamber with a more conventional chamber showed differences within 2.5% for the total and 6% for the radiation efficiencies between 1 and 6 GHz for all measured antennas.

### B. MEASUREMENT RESULTS

The antennas' measured reflection S-parameter magnitudes (with all other ports terminated in 50 Ω) are shown in Figure 9. As expected due to the absence of the (adaptive) matching circuit in our mock-up, the reflections from a 50 Ω system are quite high, mostly above −5 dB. In practice, the adaptive matching circuit would create a better match than seen here. In addition, the transmission lines and transitions on the adapter board likely affect these results. However, the reflections are sufficiently low to enable an energy transfer from the VNA to the reverberation chamber through the mock-up's antennas, allowing us to measure its efficiencies. In addition, we can gain some information from this graph, as it seems reasonable to assume that the antenna impedance is brought as close as possible to 50 Ω due to the impracticality of matching impedances far from the desired impedance. It may be noted that antenna 1 appears to work best just below 2 GHz, a frequency which is likely reduced to the GPS bands (around 1.6 and 1.2 GHz) using the (adaptive) matching network. Antenna 2 appears to target the LTE frequency bands below 2 GHz. In addition, antennas 3 and 4 seem to be relatively close to 50 Ω around the WiFi frequency bands (2.4 and 5 GHz). Antenna 5 appears to target wide-band operation, exhibiting two dips around 2.5 and 4.5 GHz.

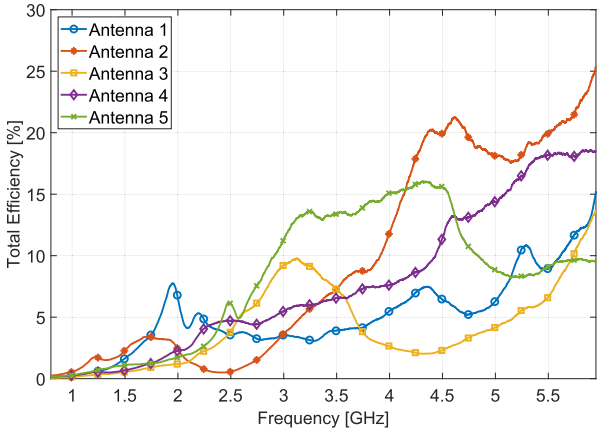


**FIGURE 10.** The measured total efficiencies of the smartphone antennas with the board. All total efficiencies are below 15% up to 4 GHz, while one of the antennas peaks to 25% up to 6 GHz. Note that this efficiency includes mismatch losses.

The total efficiency, which is not compensated for antenna mismatch, is shown in Figure 10. Antennas 1 and 2 appear to perform best below 2 GHz, peaking at nearly 8%, while the others start to pick up towards the higher frequencies. Antenna 3 performs best around 3 GHz, while

antennas 2 (sub) and 5 (main) work rather well in the at 3.5-4.5 GHz and 4-6 GHz ranges, respectively, peaking up to 15% and 20%. Note that the total efficiency is a worst-case estimate, since in the actual application an additional matching circuit is applied.

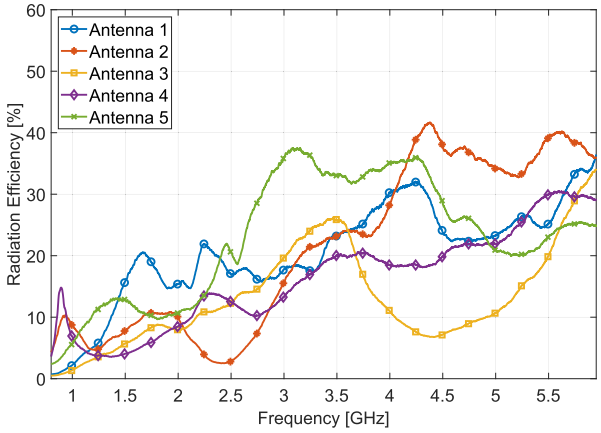


**FIGURE 11. The measured radiation efficiencies of the smartphone antennas with the board. Since the radiation efficiency does not include mismatch losses, these efficiencies are all higher than the total efficiencies. The best results in the tested frequency range peak around 40%. In the range up to 2.5 GHz the highest radiation efficiency measured is approximately 20%.**

The radiation efficiencies, shown in Figure 11, give a picture of the upper limit for the maximum achievable antenna efficiency. This efficiency can only truly be achieved assuming a perfect match, and neglects losses in the matching circuit. It can be seen that, due to the relatively high reflection coefficients to a 50 Ω system, the radiation efficiencies are considerably higher than the total efficiencies. In the frequency regime below 2.5 GHz it is interesting to note that antenna 1 indeed appears to cover GPS frequencies, peaking to approximately 20%. Nonetheless, the physical size restrictions combined with non-optimal (from an RF losses point of view) substrate material still result in mostly low efficiencies. Above 2.5 GHz the performance is significantly better, with especially antennas 2 and 5 (sub and main, respectively) together covering practically all frequencies up to 6 GHz with radiation efficiencies above 30%.

Given the extremely limited real estate, separation from the ground plane and production cost constraints, it is perhaps not surprising that the efficiencies of the antennas are not extremely high. Yet they are sufficient to achieve high performance (LTE Cat. 16) of the device. Nonetheless, an advantage in the link budget could be achieved by further improving the antennas' performance. In particular, frequency-reconfigurable antenna designs offer an interesting option to improve on the current performance in terms of efficiency [15]–[19], where radiation efficiencies above 50% and total efficiencies up to 35% have already been demonstrated using low-cost BST technology, and total efficiencies up to 63% using RF-MEMS. It also shows very clearly the challenges that lie ahead for adding more bands, as well as a key advantage of increasing operating frequency, where the antenna can be made relatively large compared to wavelength. Again, frequency-reconfigurable antennas offer an interesting solution.

## V. CONCLUSION

In this work, the efficacies of a high-end smartphone are measured to serve as a benchmark for future designs and concepts. To this end, a dedicated board is designed to facilitate connection of the antennas to the measurement system while emulating the behavior of the phone's chassis. Then, the reflection coefficients and efficiencies of the antennas are measured in a reverberation chamber. The antennas, normally connected to an adaptive matching circuit, show total efficiencies below 15% up to 4 GHz, increasing up to 25% around 6 GHz. Meanwhile, the radiation efficiencies are below 20% up to 2.5 GHz, and up to 40% for the rest of the range to 6 GHz. This type of characterization is extremely valuable to create benchmark data, and it would be of interest to repeat it for more devices in future research. Nonetheless, the efficiencies obtained here already show an opportunity to further improve performance of future devices.

## REFERENCES

[1] J. G. Andrews, S. Buzzi, C. Choi, S. V. Hanly, A. Lozano, A. C. K. Soong, and J. C. Zhang, "What will 5G be?" *IEEE J. Sel. Areas Commun.*, vol. 32, no. 6, pp. 1065–1082, Jun. 2014.

[2] *5G Vision*, DMC R&D Center Samsung Electron., Seoul, South Korea, 2015, pp. 1–16.

[3] "5G white paper," NGMN Alliance, White Paper Version 1.0, Feb. 2015. [Online]. Available: https://www.ngmn.org/uploads/media/

[4] S. Bronckers, A. Roc'h, and B. Smolders, "Wireless receiver architectures towards 5G: Where are we?" *IEEE Circuits Syst. Mag.*, vol. 17, no. 3, pp. 6–16, 3rd Quart., 2017.

[5] *NR; User Equipment (UE) Radio Transmission and Reception; Part 1: Range 1 Standalone (release 15)*, document TR38.101-1, 3GPP, 2018.

[6] N. Serafimov, P.-S. Kildal, and T. Bolin, "Comparison between radiation efficiencies of phone antennas and radiated power of mobile phones measured in anechoic chambers and reverberation chamber," in *Proc. IEEE Antennas Propag. Soc. Int. Symp.*, Jun. 2002, pp. 478–481.

[7] G. F. Pedersen, M. Tartiere, and M. B. Knudsen, "Radiation efficiency of handheld phones," in *Proc. IEEE 51st Veh. Technol. Conf.*, vol. 2. May 2000, pp. 1381–1385.

[8] O. Kivekas, J. Ollikainen, T. Lehtiniemi, and P. Vainikainen, "Bandwidth, SAR, and efficiency of internal mobile phone antennas," *IEEE Trans. Electromagn. Compat.*, vol. 46, no. 1, pp. 71–86, Feb. 2004.

[9] C.-H. Li, E. Ofli, N. Chavannes, and N. Kuster, "Effects of hand phantom on mobile phone antenna performance," *IEEE Trans. Antennas Propag.*, vol. 57, no. 9, pp. 2763–2770, Sep. 2009.

[10] Z. Ying, "Antennas in cellular phones for mobile communications," *Proc. IEEE*, vol. 100, no. 7, pp. 2286–2296, Jul. 2012.

[11] P.-S. Kildal, C. Orlenius, and J. Carlsson, "OTA testing in multipath of antennas and wireless devices with MIMO and OFDM," *Proc. IEEE*, vol. 100, no. 7, pp. 2145–2157, Jul. 2012.

[12] Z. Liu, Y. Qi, F. Li, W. Yu, J. Fan, and J. Chen, "Fast band-sweep total isotropic sensitivity measurement," *IEEE Trans. Electromagn. Compat.*, vol. 58, no. 4, pp. 1244–1251, Aug. 2016.

[13] J. Luo, E. Mendivil, and M. Christopher, "Obtaining total isotropic sensitivity from average fading sensitivity in reverberation chamber," in *Proc. IEEE Int. Symp. Antennas Propag. USNC/URSI Nat. Radio Sci. Meeting*, Jul. 2017, pp. 241–242.

[14] Y. Qi, J. Wu, Z. Zhang, L. Liu, W. Yu, A. Orlandi, J. Fan, and Z. Yang, "Objective total isotropic sensitivity measurement," *IEEE Trans. Electromagn. Compat.*, vol. 59, no. 6, pp. 1671–1676, Dec. 2017.

[15] J. R. De Luis, A. Morris, Q. Gu, and F. de Flaviis, "Tunable duplexing antenna system for wireless transceivers," *IEEE Trans. Antennas Propag.*, vol. 60, no. 11, pp. 5484–5487, Nov. 2012.

[16] P. Bahramzy, O. Jagielski, S. Svendsen, and G. F. Pedersen, "Compact agile antenna concept utilizing reconfigurable front end for wireless communications," *IEEE Trans. Antennas Propag.*, vol. 62, no. 9, pp. 4554–4563, Sep. 2014.
[17] P. Yang, K. Yan, F. Yangl, L. Y. Zeng, and S. Huang, "Reconfigurable slot antenna design for 5G smartphone with metal casing," in *Proc. IEEE Int. Symp. Antennas Propag. USNC/URSI Nat. Radio Sci. Meeting*, Jul. 2018, pp. 453–454.
[18] L. A. Bronckers, A. Roc'h, and A. Smolders, "A new design method for frequency-reconfigurable antennas using multiple tuning components," *IEEE Trans. Antennas Propag.*, to be published.
[19] X. Zhang, Y. Li, W. Wang, and W. Shen, "Ultra-wideband 8-port MIMO antenna array for 5g metal-frame smartphones," *IEEE Access*, vol. 7, pp. 72273–72282, 2019.
[20] C. L. Holloway, H. A. Shah, R. J. Pirkl, W. F. Young, D. A. Hill, and J. Ladbury, "Reverberation chamber techniques for determining the radiation and total efficiency of antennas," *IEEE Trans. Antennas Propag.*, vol. 60, no. 4, pp. 1758–1770, Apr. 2012.
[21] *Technical Specification Group Radio Access Network; Evolved Universal Terrestrial Radio Access (E-Utra); User Equipment (UE) Radio Transmission and Reception (Release 13)*, document TS 36.101 v13.2.1, 3GPP, 2016.
[22] J. L. Hilbert, *Tunable RF Components and Circuits: Applications in Mobile Handsets*. Boca Raton, FL, USA: CRC Press, 2015.
[23] D. M. Pozar, *Microwave Engineering*, 4th ed. Hoboken, NJ, USA: Wiley, 2012.
[24] P. Vainikainen, J. Ollikainen, and O. Kivekas, and I. Kelander, "Resonator-based analysis of the combination of mobile handset antenna and chassis," *IEEE Trans. Antennas Propag.*, vol. 50, no. 10, pp. 1433–1444, Oct. 2002.
[25] M. Cabedo-Fabres, E. Antonino-Daviu, A. Valero-Nogueira, and M. F. Bataller, "The theory of characteristic modes revisited: A contribution to the design of antennas for modern applications," *IEEE Antennas Propag. Mag.*, vol. 49, no. 5, pp. 52–68, Oct. 2007.
[26] A. Cabedo, J. Anguera, C. Picher, M. Ribo, and C. Puente, "Multiband handset antenna combining a PIFA, slots, and ground plane modes," *IEEE Trans. Antennas Propag.*, vol. 57, no. 9, pp. 2526–2533, Sep. 2009.
[27] *Electromagnetic compatibility (EMC) - Part 4-21: Testing and measurement techniques—Reverberation chamber test methods*, document IEC 61000-4-21:2011, Int. Electrotechn. Commision, Geneva, Switzerland, 2011.
[28] M. Piette, "Antenna radiation efficiency measurements in a reverberation chamber," in *Proc. Asia–Pacific Radio Sci. Conf.*, Aug. 2004, pp. 19–22.
[29] P.-S. Kildal and K. Rosengren, "Correlation and capacity of MIMO systems and mutual coupling, radiation efficiency, and diversity gain of their antennas: Simulations and measurements in a reverberation chamber," *IEEE Commun. Mag.*, vol. 42, no. 12, pp. 104–112, Dec. 2004.
[30] A. Azremi, H. G. Shiraz, and P. S. Hall, "Reverberation chamber for efficiency measurement of small antennas," in *Proc. 1st Int. Conf. Comput., Commun., Signal Process. Special Track Biomed. Eng.*, Nov. 2005, pp. 25–29.
[31] C. S. Lee, A. Duffy, and C. Lee, "Antenna efficiency measurements in a reverberation chamber without the need for a reference antenna," *IEEE Antennas Wireless Propag. Lett.*, vol. 7, pp. 448–450, 2008.
[32] A. Khaleghi, "Time-domain measurement of antenna efficiency in reverberation chamber," *IEEE Trans. Antennas Propag.*, vol. 57, no. 3, pp. 817–821, Mar. 2009.
[33] H. G. Krauthäuser and M. Herbrig, "Yet another antenna efficiency measurement method in reverberation chambers," in *Proc. IEEE Int. Symp. Electromagn. Compat.*, Jul. 2010, pp. 536–540.
[34] Q. Xu, Y. Huang, X. Zhu, L. Xing, Z. Tian, and C. Song, "A modified two-antenna method to measure the radiation efficiency of antennas in a reverberation chamber," *IEEE Antennas Wireless Propag. Lett.*, vol. 15, pp. 336–339, 2015.
[35] D. Senic, D. F. Williams, K. A. Remley, C.-M. Wang, C. L. Holloway, Z. Yang, and K. F. Warnick, "Improved antenna efficiency measurement uncertainty in a reverberation chamber at millimeter-wave frequencies," *IEEE Trans. Antennas Propag.*, vol. 65, no. 8, pp. 4209–4219, Aug. 2017.
[36] R. Serra, A. C. Marvin, F. Moglie, V. M. Primiani, A. Cozza, L. R. Arnaut, Y. Huang, M. O. Hatfield, M. Klingler, and F. Leferink, "Reverberation chambers a la carte: An overview of the different mode-stirring techniques," *IEEE Electromagn. Compat. Mag.*, vol. 6, no. 1, pp. 63–78, 1st Quart., 2017.
[37] *Double-Ridged Waveguide Horn Antennas Datasheet*, ETS-Lindgren, Cedar Park, TX, USA.
[38] *Double Ridge Horn AH-118 Datasheet, Revision d10.15*, Com-Power Corp., Silverado, CA, USA.

**LAURENS A. BRONCKERS** received the M.Sc. degree *(cum laude)* in electrical engineering from the Eindhoven University of Technology (TU/e), in 2015, where he is currently pursuing the M.Sc. degree, with a focus on frequency-reconfigurable antenna design for mobile applications and antenna measurement techniques. He was a Guest Researcher with the National Institute of Standards and Technology (NIST), in 2018. He is currently with the Electromagnetics Group, TU/e, to pursue further advances in RF measurement techniques, with a focus on reverberation chamber methods.

**ANNE ROC'H** (M'07) received the M.Sc. degree in electronics and telecommunications from the École Nationale d'Ingénieurs de Limoges, Limoges, France, in 2005, and the Ph.D. degree in electrical engineering from the University of Twente, Enschede, The Netherlands, in 2012. From June 2010 to March 2011, she was with the University of Eindhoven, Eindhoven, The Netherlands, where she worked on computational electromagnetics. She was an EMC Expert in the industry, from March 2011 to June 2014. Since then, she has been an Assistant Professor of electromagnetic compatibility with the University of Eindhoven.

**A. BART SMOLDERS** was born in Hilvarenbeek, The Netherlands, in 1965. He received the M.Sc. and Ph.D. degrees in electrical engineering from the Eindhoven University of Technology (TU/e), in 1989 and 1994, respectively. From 1989 to 1991, he was an IC Designer with FEL-TNO, The Hague. From 1994 to 1997, he was a Radar System Designer with Thales, The Netherlands. From 1997 to 2000, he was the Project Leader of the Square Kilometer Array (SKA) with the Netherlands Foundation for Research in Astronomy (ASTRON). From 2000 to 2010, he was with NXP (formerly Philips) Semiconductors, The Netherlands, where he was responsible for the innovation in the RF business line. Since 2010, he has been a full-time Professor with the Electromagnetics Group, TU/e, with special interest in antenna systems and applications. He is also the Dean of the Electrical Engineering Department, TU/e. He has published more than 140 papers. He currently leads several research projects in the area of integrated antenna systems operating at frequencies up to 120 GHz for several application domains, including 5G/6G wireless communications, radar sensors, and radio-astronomy. He is also a Board member of the Stichting Wetenschappelijke Activiteiten van het Nederlands URSI Committee (SWAN) and a member of the Advisory Board of ASTRON. He is also the Junior-Past Chairman of the IEEE Benelux section and the Past-Chair of the NERG (Nederlands Radio-en Elektronica Genootschap).